Structural Development of Poly(ethylene terephthalate) During Uniaxial Stretching Above the Glass-Transition Temperature: Study of the Statistical Influence of the Stretching Variables

Lyudmil V. Todorov, Carla I. Martins, Júlio C. Viana

Department of Polymer Engineering, Institute for Polymers and Composites/I3N, University of Minho, Campus Azurãm, 4800-058 Guimarães, Portugal

Received 18 January 2010; accepted 27 July 2010
DOI 10.1002/app.33099
Published online 11 November 2010 in Wiley Online Library (wileyonlinelibrary.com).

ABSTRACT: In this article, we present an investigation of the structural development of poly(ethylene terephthalate) (PET) during uniaxial stretching above the glass-transition temperature; this followed a statistical design of experiment approach to determine the influence of the stretching variables on the structural development. Amorphous PET was submitted to a stretching program with variations in the stretching temperature (T_{st}), stretching rate ($\dot{\varepsilon}_{st}$), and stretching ratio (λ_{st}). Stretched samples were rapidly quenched and characterized by wide-angle X-ray scattering, optical birefringence, and differential scanning calorimetry. The relevance and influence of the stretching variables on the obtained parameters (phase fraction, phase orientation, and thermal parameters) were analyzed. The strain-induced crystallinity was controlled by T_{st}, λ_{st}, and the interactions between them. Mesophase development was not dependant on T_{st} but on the interactions between $\dot{\varepsilon}_{st}$ and λ_{st}. The molecular orientation was proportionally dependent on T_{st}, λ_{st}, and their interactions. © 2010 Wiley Periodicals, Inc. J Appl Polym Sci 120: 1253–1265, 2011

Key words: differential scanning calorimetry (DSC); drawing; orientation polyesters; WAXS

INTRODUCTION

Poly(ethylene terephthalate) (PET) is a thermoplastic polyester of important commercial significance because of its enhanced mechanical, thermal, and barrier properties. It is a slowly crystallizing material that can have different degrees of crystallinity (χ_c's) when it is cooled from the melt, depending on the cooling rate applied. Therefore, it can be either in a semicrystalline state or in an amorphous state, the last when it is rapidly quenched from the melt. Amorphous PET can be further crystallized if deformed in the rubbery state, that is, above its glass-transition temperature (T_g).[1] The distinguishing feature of PET to develop a specific semicrystalline microstructure under uniaxial stretching in the rubbery state plays an important role in the performance and characteristics of the final products.

PET's structural development is directly related to the thermomechanical environment used during uniaxial stretching. Many studies have been conducted to characterize this material under different stretching conditions and to relate those to its structural development.[2–7] Different techniques were used, from postmortem techniques based on densiometric measurements,[8–10] fluorescence spectroscopy,[10–14] Raman spectroscopy,[15,16] IR spectroscopy,[11,17–22] X-ray diffraction,[3–6,8,11,17,18,22–30] optical birefringence (BIR),[3,6,10,16,17,30–34] and differential scanning calorimetry (DSC)[6,7,20,25,30,35] to *in situ* characterization with synchrotron X-ray diffraction,[20,36–43] online BIR,[7] and real-time Fourier transform infrared spectroscopy.[44] These studies allowed significant progress on the understanding of structural formation in PET films and fibers. The mechanical response and structural development were correlated by Salem,[8,9] which divided this process into two stages: (1) the initial stage, where the stress increased slowly with stretching ratio (λ_{st}) but the crystallinity increased relatively fast (up to 15% crystallinity), and (2) second stage, where the stress increased rapidly (strain

Correspondence to: J. C. Viana (jcv@dep.uminho.pt).

Contract grant sponsor: DESY and the European Commission under HASYLAB Project DESY-D-II-05-101 EC and the FP6 contracts RII3-CT-2004-506008 IA-SFS.

Contract grant sponsor: Project APT_PACK-SRTP-505204-1.

Contract grant sponsor: Portuguese Foundation for Science and Technology; contract grant number: SFRH/BD/44917/2008 (a Ph.D. student grant).

hardening) and the crystallinity increased slowly. Gorlier et al.[29] investigated the rubbery-state deformation of initially amorphous PET by WAXS. They suggested a three-stage structural development mechanism consisting of (1) orientation (molecular orientation occurred because of strong molecular interactions), (2) nucleation (nuclei appeared as a result of molecular orientation and at a given level of strain, the number of nuclei was fixed; this formed a network structure that was responsible for strain hardening), and (3) a growth stage (crystallization developed through the growth process). Kawakami and coworkers,[43,45] by *in situ* WAXS and small-angle X-ray scattering (SAXS), provided new insights to the subject by determining that the first stage, also called the *orientation stage*, would take place until strain hardening was initiated (plastic deformation region) and involved the formation of a mesophase with highly oriented chain segments. In this stage, the oriented mesophase increased continuously with the applied strain without the formation of crystals. The appearance of an equatorial streak in SAXS patterns at the later phase of the stage indicated the formation of a microfibrillar structure. The second stage, nucleation, involved the initiation of crystallization from the mesophase through nucleation and growth processes. This stage occurred during the strain-hardening region. Imperfect crystals (second order crystals) were observed for strains up to the initiation of strain hardening. Increasing strain was followed by further chain orientation and crystal perfection. SAXS analysis showed the existence of two substages within the nucleation stage: (1) the formation of a titled lamellar structure within the microfibrils in conjunction with lamellar insertion and (2) lamellar insertion, which occurred at a slower rate. The last stage, growth, corresponded to the stable crystal (third order crystals) growth phase, where the lamellar superstructure was responsible for the linear load increase with strain, which enabled a good lattice PET triclinic unit cell to be registered in the WAXS patterns. However, at very high strains, some lamellar domains became fragmented; this resulted in microfibrillar spinning and was the prelude for catastrophic disruption of the crystalline phase.

Martins and Cakmak[7] proposed three-stage stress–optical behavior for the structural development of amorphous PET above T_g on the basis of *in situ* BIR measurements simultaneous with the mechanical stretching of PET films and *ex situ* WAXS and DSC analyses. In the early stages of deformation, a linear increase in the birefringence (Δn) with stress was observed; this followed the stress–optical rule, whereas the material remained in the amorphous stage. Then, a fast increase in Δn was observed at almost constant stress. Here, there was the formation of crystalline structures with the establishment of a long-range connected network. With further deformation, the chains connected through the network approached their finite extensibilities (third stage). In this stage Δn achieved a plateau, whereas the stress increased with strain hardening.

The phases were defined by Ajji and coworkers,[17,18] using Fourier transform infrared spectroscopy, as (1) an amorphous phase, composed solely of gauche conformers; (1) a mesophase, consisting of gauche and highly oriented trans conformers; and (3) a crystalline phase, consisting only of trans conformers. The mesophase has been the focus of many studies. Blundell and coworkers,[37,38,46] by *in situ* WAXS, concluded that when fast rates are applied, crystallization does not appear during the stretching process. Instead, a mesomorphic structure appears; this is the precursor of the crystalline structures that appear when stretching has been finished. These observations were based on the disappearance of the meridional (00-1) peak at $2\theta = 8.56^\circ$ and the simultaneous appearance of the triclinic crystalline peak at the equator. Ran et al.,[47] via *in situ* WAXS, indicated that the mesophase was developed during deformation, as detected by an intensity increase when the meridian peak (00-1) was stretched (d = 10.32 Å); this corresponded to an inclined smectic C structure. This peak drastically decreased when the crystalline structure started to appear. Asano et al.[48] suggested the formation of oriented nematic structures upon the solid-state stretching of amorphous PET, with alternate positioning of the phenylene rings on neighboring molecules. After annealing to 60°C, the nematic phase transforms into smectic, with the neighboring rings aligned on the plane perpendicular to the stretching direction and a slight tilt of the molecules. Kawakami et al.[49] proposed the formation of a mesophase in the early stages of deformation. The mesophase has a degree of packing order between the crystalline phase and the amorphous phase. According to the authors, the mesophase is responsible for the nucleation and formation of imperfect crystals (with second order) and forms a network and causes strain hardening to occur.

Some studies,[29,50] dealing particularly with the influence of stretching variables on the molecular orientation, indicated that the orientation level increased with increasing stretching rate ($\dot{\varepsilon}_{st}$) and decreasing temperature. Other researchers have focused on the effects of the stretching variables on the crystallinity and suggested that crystallinity develops above $\lambda_{st} = 2.0$,[9,17,20,51,52] but its appearance can occur at higher strains with increasing stretching temperature (T_{st}) and/or decreasing $\dot{\varepsilon}_{st}$.[8,9,14,29,53]

Despite the abundant number of investigations in this area, there is still a lack of understanding of the contribution and influence of each stretching

TABLE I
Stretching Program According to an L8 Taguchi Orthogonal Array

Variable		Condition							
		C1	C2	C3	C4	C5	C6	C7	C8
Temperature (°C)	T_{st}	90	110	90	110	90	110	90	110
Rate (s^{-1})	$\dot{\varepsilon}_{st}$	0.003	0.003	0.03	0.03	0.003	0.003	0.03	0.03
Ratio[a]	λ_{st}	1.6	1.6	1.6	1.6	2.1	2.1	2.1	2.1

[a] $\lambda_{st} = (l_0 + d)/l_0$, where l_0 is the initial length of rectangular part of the tensile bar and d is the displacement.

parameter on the structural development of PET during uniaxial stretching in the rubbery state. In this investigation, we aimed to go further into this subject by applying an experimental protocol consisting of the variations of T_{st}, $\dot{\varepsilon}_{st}$, and λ_{st} and analyzing their statistical contributions to the strain-induced structure of PET. The relevance and influence of the stretching variables on the development of the phase fraction, orientation, and thermal parameters are discussed.

EXPERIMENTAL

Material

The PET used in this study was supplied by Tergal Fibers S. A. (Gauchy, France) and had an intrinsic viscosity of 0.74 ± 0.02 dL/g (bottle grade), a solid density of 1.40 g/cm^3, and an approximate average molar mass of 20,000 g/mol.

Samples preparation

Compression-molded plaques with dimensions of 200 × 200 × 0.3 mm^3 were prepared from dried PET pellets (they were dried at 170°C for 4 h in a dry-air atmosphere according to manufacturer recommendations) under the following conditions: the material was heated to 285°C for 5 min with no pressure. The pressure was increased to 774 MPa and then released; this cycle was repeated three times to ensure that the samples were free of air bubble. Finally, the material was held at 774 MPa for 5 min and rapidly quenched in a water vessel adapted with a cooling device to control the temperature at −5 ± 0.5°C and to obtain amorphous PET samples. In this article, we call these samples the *as-molded samples*.

Dumbbell-like specimens (length = 95 mm, cross section = 42 × 0.3 mm^2) were cut from the compression-molded plaques. These samples were stretched in a universal tensile testing machine (Instron 4505, Grove City, PA, USA) equipped with an environmental chamber with the stretching program presented in Table I. The stretching procedure included variations in T_{st}, $\dot{\varepsilon}_{st}$, and λ_{st} within the limits of the stretching equipment, according to a L8 Taguchi orthogonal two-level array.[54]

Samples were clamped at room temperature at a gauge length of 55 mm and then heated to the programmed temperature by circulating hot air in the environmental chamber. Before stretching, samples were allowed to thermally equilibrate for 2 min. After stretching, the samples were maintained clamped, whereas high-pressure CO_2 at −70°C was introduced into the chamber to uniformly cool the sample and the entire testing instrument (clamps and chamber); we did this with the intention of diminishing the heat transfer among the hot metallic grips and the polymeric sample.

Wide-angle X-ray scattering (WAXS)

WAXS patterns were obtained with an X-ray synchrotron radiation beam monochromized by the reflection of a bent Ge (111) single crystal (λ = 0.15 nm). These experiments were carried out at HASYLAB, DESY (Hamburg, Germany), on an A2 soft condensed matter beamline. The specimens were positioned perpendicularly to the incident X-ray beam with the stretching direction pointing vertically. For all of the experiments, the sample-to-detector distance was set at 13.5 cm. The second-order WAXS patterns were acquired with a MARCCD camera with an accumulation time of 20 s. Calibration was carried out with homemade, from the laboratory, standard PET crystalline sample. Background scattering was subtracted, and all plots were normalized with respect to the incident X-ray intensity.

A peak-fitting program was used to deconvolute the crystalline peaks, and the amorphous halo from the intensity profiles was extracted from the second-order WAXS patterns. The pattern treatment was adapted from that proposed by Kawakami et al.[49] The equatorial and meridional profiles of the second-order WAXS patterns were used to estimate the mass fractions of the three phases: the amorphous phase, mesophase (which had a degree of packing between those of the crystalline and amorphous phases), and crystalline phase. The amount of the crystalline phase was assumed to be proportional to the total area of the deconvoluted peaks: (010) at 2θ = 17.3°, (−110) at 2θ = 22.5°, and (100) at 2θ = 25.7° were taken from the linear equatorial profile, whereas the amount of unoriented amorphous phase

was assumed to be proportional to the area of the linear meridional profile. When a crystal diffraction peak was detected in the meridional profile [e.g., at (−103) at 2θ = 26.6° reflection], its area contribution was excluded (e.g., C7).[43] The subtraction of the crystalline and amorphous fractions from the total area of the equatorial profile was considered to be proportional to the amount of the mesophase. The mass fraction of the individual phases was taken to be the ratio of the area for each phase to the total area of the equatorial profile.

To calculate the average polymer orientation (f_{av}), WAXS patterns were integrated along an azimuthal angle of μ = 0–π/2 over a section with 2θ = 13–28°. This sector enclosed all possible crystal reflections of the crystallographic planes, isotropic amorphous phase, and mesophase of PET.[5] Herman's orientation function was used to evaluate f_{av}, which was calculated by the following equation:[55]

$$f_{av} = \frac{3\langle \cos^2 \phi \rangle - 1}{2} \tag{1}$$

where $\langle \cos^2 \phi \rangle$ is defined as

$$\langle \cos^2 \phi \rangle = \frac{\int_0^{\pi/2} I(\phi) \cos^2 \phi \sin \phi d\phi}{\int_0^{\pi/2} I(\phi) \sin \phi d\phi} \tag{2}$$

where φ is the azimuthal angle with respect to the equator (φ = 0), I the diffracted intensity and cos φ the average angle that the normal makes with principal deformation direction.

Additionally, the amorphous-phase orientation (f_{am}) was determined from azimuthal scans obtained over μ = 2π between 2θ values of 19.3 and 20.8°.[25] This annular ring was located between (010) at 2θ = 17.3° and (−111) at 2θ = 21.2° crystalline reflections, that is, at an angular range where the amorphous peak was reasonably intense and had the least overlap with the crystalline reflections when such were present. The profiles were fitted to Gaussian peaks and a horizontal baseline. The width of the peak was used to calculate f_{am} with Herman's equations [eqs. (1) and (2)]. $\langle \cos^2 \phi \rangle$ was evaluated by the full width at half-maximum (Δφ) of the Gaussian peak intensity distribution by $\langle \cos^2 \phi \rangle$ integrated between π/2 and −π/2 for each value of Δφ from the following relationship:

$$I(\phi) = \exp\left(\frac{-4\phi^2 \ln 2}{\Delta\phi^2}\right) \tag{3}$$

BIR

In-plane BIR measurements were obtained with a commercially available spectrophotometer (Shimadzu UV-2401PC ultraviolet–visible spectrophotometer) modified to accommodate the polarizer–sample–analyzer system. The measurements were performed within the wavelength (λ) range 350–800 nm. The polarizer–sample–analyzer sandwich was interposed in the spectrophotometer system, and transmittance (T) versus λ graphs were obtained. The methodology used to determining Δn was the following:[56] the phase difference (δ) as a function of λ was defined as follows:

$$\delta = \frac{2\pi\Gamma}{\lambda} \tag{4}$$

where Γ is the retardation and could be written as follows:

$$\Gamma = m\lambda = d \times \Delta n \tag{5}$$

In this equation, m is an integer when the condition of constructive interference is met and the emergent light is plane polarized, and d is the thickness of the specimen. If one defines $m = \frac{\delta}{2\pi}$, Eq. (5) becomes

$$m = \frac{d \times \Delta n}{\lambda} \tag{6}$$

Thus, by plotting m versus $1/\lambda$, ($d \times \Delta n$) can be readily determined by the slope of the linear portion of the curve. Because d is known, Δn can be calculated.

DSC

A PerkinElmer DSC-7 instrument (Waltham, Massachusetts, USA) running in standard mode was used. The temperature of the cold block was kept at 5°C, and the nitrogen purge gas flow rate was 20 cm^3/min. The temperature and enthalpic calibrations were carried out with indium and lead standards. Heating experiments were performed for all of the samples from 30 to 270°C at a heating rate of 20°C/min. The sample weight was around 9 mg.

T_g and the cold crystallization and melting parameters were obtained from the heating scans. The melting temperature (T_m) and cold crystallization temperature (T_{cc}) were considered to be the maximum values of the endothermic and exothermic peaks, respectively. The enthalpy of fusion (ΔH_m) and the enthalpy of cold crystallization (ΔH_{cc}) were determined from the areas of T_m and the crystallization peak, respectively. The calculation of χ_c was based on a two-phase (crystalline–amorphous) method with the following equation:

$$\chi_c = \frac{\Delta H_m - \Delta H_{cc}}{\Delta H_f} \tag{7}$$

TABLE II
Structural Parameters of As-Molded PET

Sample	Amorphous-phase fraction (%)	Mesophase fraction (%)	f_{av}	f_{am}	BIR
As-molded PET	96.5	3.5	−0.15	−0.30	0.008

where ΔH_f is the enthalpy of fusion of pure PET crystals and was taken to be equal to 120 J/g.[57] The reported results are the average of the measurements obtained in three different samples.

Statistical data treatment

The experimental stretching program was defined with a Design of Experiment (DOE) approach. Analysis of variance was performed on all assessed structural and thermal parameters.[58] The use of a DOE and data analysis by analysis of variance allowed the independent assessment of the influence of each individual factor and its interactions (that could not be assessed by the traditional approaches of varying the stretching parameters one at one time). The results presented were significant with a 95% confidence limit. The statistical significance of the stretching parameters (factors) was evaluated by the *F*-ratio and translated into a percentage of contribution of the individual factor and factor interactions. The influence of the stretching variables and their interactions is presented in effect graphs.

RESULTS AND DISCUSSION

As-molded PET

As-molded PET samples were characterized in terms of WAXS, BIR, and DSC to access the structural state of the material. The results are summarized in Table II. The analyses of the second-order WAXS patterns indicated a content of 96.5% of amorphous material. f_{av} and f_{am} were −0.15 and −0.30, respectively; this indicated that the polymer chain tended to orient perpendicularly to the stretching (equatorial) direction. This result was caused by the compression-molding procedure. The BIR measurement showed a Δn level of 0.008; this value was recognized as belonging to a fully isotropic state.[3] DSC showed a residual crystallinity level of less than 5%, which is typical for amorphous PET.[58] We concluded from these results that the compression-molded samples obtained were amorphous.

Stretched PET samples

Structural characterization by WAXS and BIR

The second-order WAXS patterns of the stretched samples are presented in Figure 1. Only two sets of conditions developed a crystalline pattern; these were conditions C5 and C7. These samples were stretched at the lowest temperature (90°C) and at the highest λ_{st} applied (2.1×) at both studied $\dot{\varepsilon}_{st}$ values. All of the other conditions gave rise to an amorphous halo, although in some cases, the intensity profile seemed to concentrate at the equator region; this suggested the existence of some polymer chain orientation in the stretching direction and the

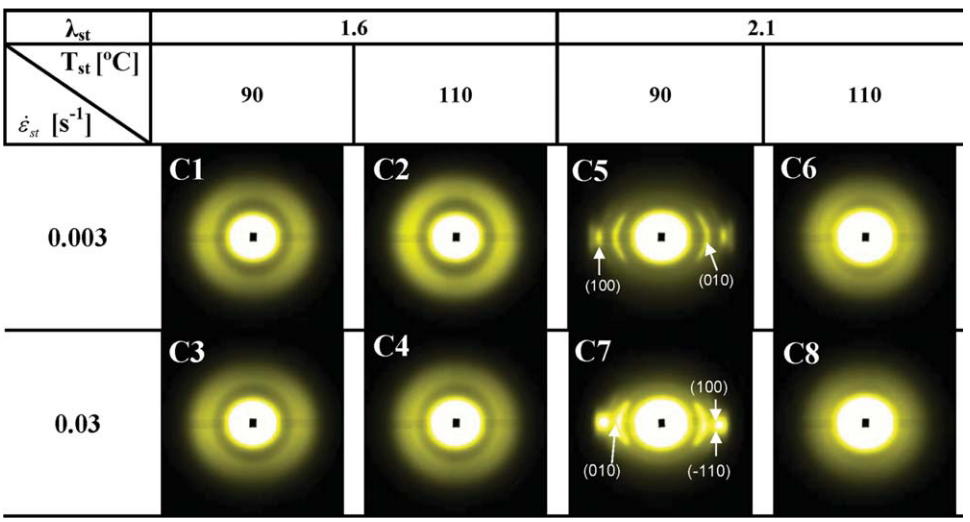

Figure 1 WAXS patterns of PET samples stretched in the rubbery state. [Color figure can be viewed in the online issue, which is available at wileyonlinelibrary.com.]

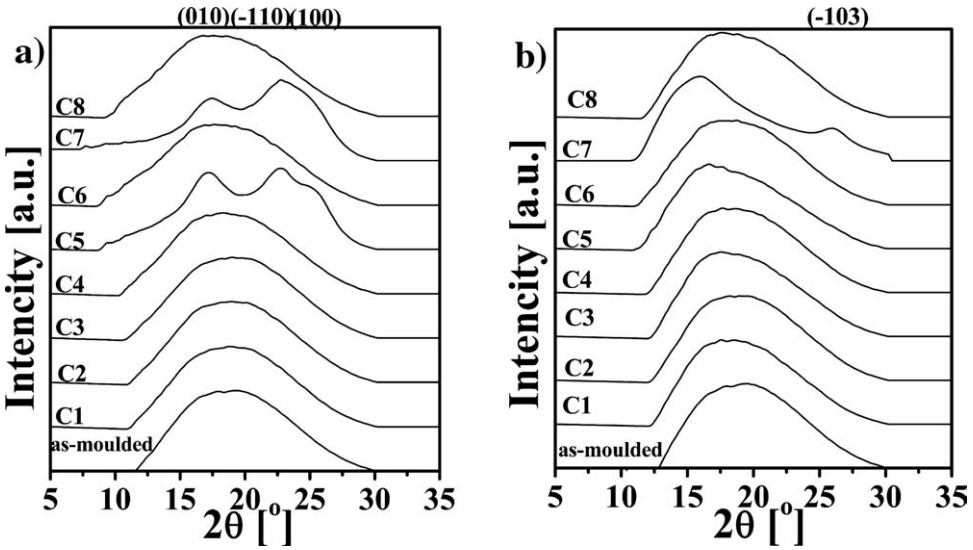

Figure 2 (a) Equatorial and (b) meridional linear intensity profiles extracted from second-order WAXS patterns.

presence of some content of mesophase, as reported elsewhere.[39,43,45,47,49] Although we expected to have amorphous halos in the C1, C2, C3, and C4 conditions, because the material was stretched to only 1.6×, C6 and C8 were stretched to a much higher stretching level (2.1×) and still presented amorphous halos. This result showed that the temperature had an important role in the structural development of the sample, and in these cases, it hindered the strain-induced crystallization mechanism of PET because of a possible competing mechanism between chain elongation due to mechanical deformation and chain relaxation due to the elevated temperature.

To detail the morphological state of the samples obtained in each condition, the equatorial and meridional intensities versus the 2θ profiles extracted from the second-order WAXS patterns were analyzed. These results are shown in Figure 2. As shown in Figure 2(a), three distinct equatorial reflection peaks were identified for samples C5 and C7, namely (010) at $2\theta = 17.3^\circ$, (−110) at $2\theta = 22.5^\circ$, and (100) at $2\theta = 25.7^\circ$. These peaks corresponded to the lattice planes parallel to the molecular *c* axis of the PET triclinic unit cell.[5] In the case of C7, (−110) was overlapped with the (100) reflection, and therefore, it was difficult to identify it. When looking at the meridional intensity profiles [Fig. 2(b)], we observed a small crystalline reflection, assigned to the crystalline unit cell reflection (−103) at about $2\theta = 26.3^\circ$, in the C7 sample only. According to Kawakami et al.,[49] this peak is visible during the so-called nucleation stage, but it is not located in the meridional position until the beginning of the growth stage. An increase in the orientation and crystal perfection caused the shifting of the (−103) peak to the meridian as a result of third-order crystalline formation. This peak was not observed for the C5 sample; this indicated that an imperfect second-order crystalline phase was obtained under these conditions (lower strain rate compared to C7).

All of the other cases showed typical broad amorphous peaks. Nevertheless, the dissimilarities in the shape and area of the meridional intensity versus 2θ profiles [Fig. 2(b)] indicated the presence of dissimilar amorphous mass fractions.

From the second-order WAXS patterns shown previously, the mass fractions of the amorphous, mesophase, and crystalline phases were estimated. The results are presented in Figure 3(a). Shown in Figure 3(b) are f_{am} and f_{av} calculated through the use of Herman's orientation function. In the same plot, the polymer orientation obtained through BIR measurements is shown.

As shown in Figure 3(a), the samples deformed at lower λ_{st} ($\lambda_{st} = 1.6$) and lower $\dot{\varepsilon}_{st}$ ($\dot{\varepsilon}_{st} = 0.003\ s^{-1}$), respectively, C1 and C2, had the highest amount of amorphous-phase fraction among the studied conditions. They showed around 90% amorphous-phase fraction and 10% mesophase fraction for both temperatures used. The increase in $\dot{\varepsilon}_{st}$ (C3 and C4) caused a decrease in the amorphous phase and an increase in the mesophase fraction; this was slightly more pronounced when a low temperature was used (C3). According to the results shown in Figure 3(b), samples stretched to low λ_{st} values, C1–C4, had similar levels of orientation; these increased slightly when $\dot{\varepsilon}_{st}$ increased (i.e., C1 and C3) or T_{st} decreased (i.e., C2 and C1 or C4 and C3). For instance, sample C3 stretched at a high rate and at a lower temperature had 11.5% less amorphous phase, and it was better oriented according to the f_{am} results than sample C4 [Fig. 3(b)].

When high λ_{st} values were applied (C5 to C8), two different morphologies were detected. For high

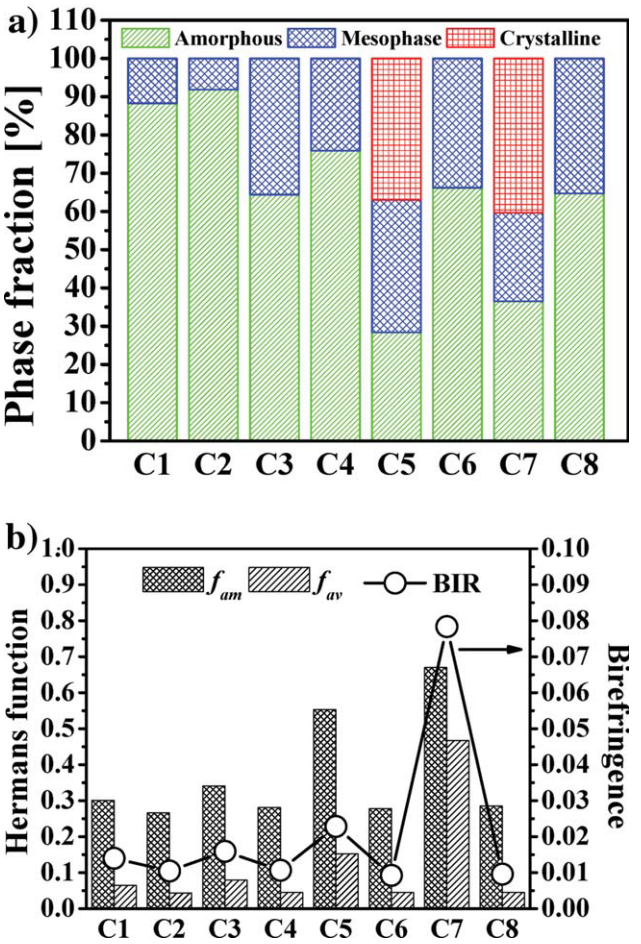

Figure 3 (a) Percentage of mass fractions and (b) f_{am} and f_{av} values calculated from second-order WAXS patterns and polymer chain orientations determined by Δn measurements. [Color figure can be viewed in the online issue, which is available at wileyonlinelibrary.com.]

temperatures (C6 and C8), the material was composed of around 65% amorphous-phase fraction and 35% mesophase fraction; this was independent of the strain rate applied [Fig. 3(a)]. For low temperatures, the material crystallized, showing a reduction in the amorphous-phase and mesophase fractions and the appearance of a crystalline phase. These two conditions (C5 and C7) showed the highest levels of amorphous and average orientation function among all of the conditions. The effect of strain rate was mostly observed here, where C7, corresponding to a deformation with higher $\dot{\varepsilon}_{st}$, appeared with much higher levels of amorphous orientation and f_{av}, compared to C5.

From the results shown in Figure 3(a), it was also possible to observe the importance of the strain ratio on the development of the crystalline structures. This processing variable had a pronounced influence on the strain-induced crystalline phase when low temperatures were applied, for both $\dot{\varepsilon}_{st}$ values used, as observed when the samples obtained at low $\dot{\varepsilon}_{st}$ values (C1 and C5) and at high $\dot{\varepsilon}_{st}$ values (C3 and C7) were compared. The results suggest that decreased T_{st} facilitated the strain-induced structural development, and an identical but minor effect was given by the elevated $\dot{\varepsilon}_{st}$ values. This conclusion was also put forward by other authors.[59]

In general, low λ_{st} resulted in a low average polymer chain orientation, as observed by Δn measurements and by the average orientation function, presented in Figure 3(b). With regard to the amorphous phase, some level of orientation was observed, which was slightly higher for the samples stretched at lower temperatures (C1 and C3).

The combination of high λ_{st} and high temperature resulted in samples with similar orientation levels as those previously described. Although the orientation level was the same, the elevated λ_{st} seemed to have a positive influence on the transformation of the amorphous-phase fraction into the mesophase (cf. C2–C6 and C4–C8). At high temperatures, the polymer orientation and polymer relaxation were competing mechanisms[60] and, thus, hindered the samples from crystallizing. For low T_{st} values (C5 and C7), the samples showed less amorphous phase, a dissimilar amount of mesophase, and the presence of the crystalline phase. Although C7 had a faster $\dot{\varepsilon}_{st}$, it appeared with less mesophase mass fraction than C5 [Fig. 3(a)]. This might be explained as follows: the applied fast rate caused an increase in mesophase but, because this phase was responsible for nucleation and the formation of imperfect crystals (second-order crystallites), which started forming a network, this mesophase was easily converted into the crystalline phase. As observed, this sample had slightly more crystalline phase than sample C5. The crystalline phase of C7 was third order, whereas in C5, it consisted of an imperfect crystalline phase with second order. In terms of orientations [Fig. 3(b)], the results presented much higher levels of f_{am}, f_{av}, and Δn compared to those of the other studied conditions.

Thermal characterization by DSC

Figure 4 depicts the DSC thermograms of the as-molded sample and the stretched counterparts. As observed, different structural states were evidenced by the DSC thermograms. The samples stretched at high temperatures (C2, C4, C6, and C8) had identical DSC curves as the as molded plate. They showed a broad T_{cc} peak with a maximum around 147°C. These samples had an χ_c below 5%, as shown in Table III; therefore, one can consider that they were in the amorphous state. When a lower T_{st} was applied, two different results appeared; this depended on λ_{st}. For low λ_{st}, that is, C1 and C3, the T_{cc} peak narrowed and moved slightly toward T_g, appearing around

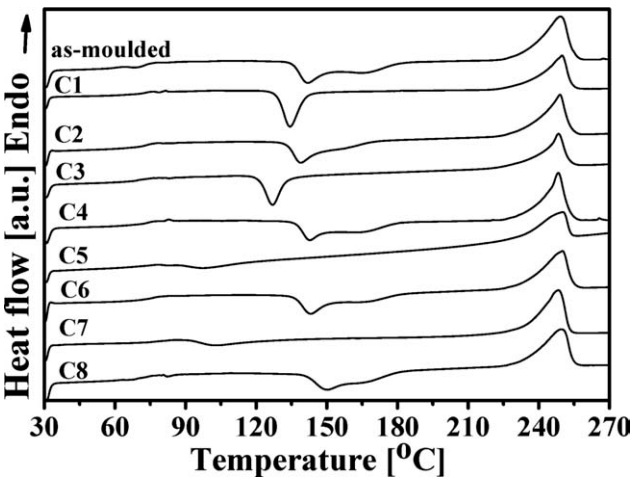

Figure 4 DSC thermograms obtained at a heating rate of 20°C/min.

135°C. In this case, χ_c increased slightly to values between 5 and 12%, also considered a quasi-amorphous state. The biggest change was observed for C5 and C7, where a high λ_{st} was applied. In this case, T_{cc} overlapped with the glass transition, appearing around 100°C. These samples had around 28 and 32% crystallinity. The movement of T_{cc} toward the glass transition indicated that the chains were more oriented compared to those of the other samples. This result also confirmed the WAXS results shown previously.

Table III shows the results acquired from the DSC thermographs. With regard to T_g, its minimum and maximum values were observed in the range 70–80°C. These results were expected for PET samples having different percentages of crystallinity, with the lowest corresponding to amorphous samples and the highest corresponding to a more crystalline sample. The highest T_g was observed for samples C5 and C7; those samples presented the highest level of crystallinity. As Viana at al.[57] suggested, the crystalline phase geometrically constrained the amorphous phase, inhibiting the amorphous-phase motion and increasing T_g. With regard to T_m, it remained constant around 249°C for all of the conditions studied.

The different structural states of the samples were mainly evidenced in the position and area of T_{cc}. Generally, the movement of T_{cc} is a sensitive measure of the state of the polymer chains. If amorphous chains are oriented but not crystallized during the stretching process, T_{cc} decreases toward the glass transition as f_{am} increases.[25,61] A decrease in T_{cc} and ΔH_{cc} with respect to the as-molded PET was shown by all of the samples stretched at a lower T_{st} (90°C; C1, C3, C5, and C7), and an opposite effect was observed for all of the samples submitted to a higher T_{st} value (110°C). This suggested an important influence of T_{st} on the cold crystallization and, consequently, on the orientation of the amorphous phase. The developed crystalline structure caused a strong shift in the T_{cc} position toward the glass transition, as observed for C5 (e.g., 99.5°C) and C7 (e.g., 102.3°C). The more perfect crystalline structure of C7 contributed to the slightly higher value of T_{cc} compared to C5; this was attributed to the more oriented amorphous phase.

Structural interpretation

From the results analyzed previously, the following remarks can be withdrawn:

1. Conditions C1–C4 and C6 and C8 gave rise to amorphous oriented structures, also called *quasi-amorphous* structures. Although C6 and C8 were deformed to higher λ_{st}, the use of high temperatures (almost 40°C above T_g) might have promoted a process of strain relaxation that was faster than the strain orientation of the chains. This competing mechanism was also reported in the literature by other authors.[38] The absence of a crystalline phase, detected by WAXS, assigned those condition to the orientation stage of Structure Development Mechanisms (SDM).[29]
2. Condition C5 resulted in a semicrystalline structure with crystallites characterized as second order. Although a high level of crystallinity ($\sim$ 28% detected by DSC) was achieved, the average polymer chain orientation remained

TABLE III
DSC Results

Sample	T_g (°C)	T_{cc} (°C)	ΔH_{cc} (J/g)	T_m (°C)	ΔH_m (J/g)	χ_c (%)
As-molded	72.4 ± 0.2	139.9 ± 2.4	37.4 ± 1.0	248.6 ± 0.5	41.4 ± 0.7	3.3 ± 0.3
C1	73.5 ± 0.7	135.0 ± 1.4	32.5 ± 1.0	249.3 ± 0.6	41.4 ± 0.9	7.4 ± 0.7
C2	72.3 ± 0.4	140.9 ± 3.3	35.7 ± 2.0	249.3 ± 0.6	41.5 ± 1.0	5.4 ± 0.0
C3	70.8 ± 0.6	132.6 ± 3.3	28.1 ± 0.0	248.9 ± 0.6	42.3 ± 0.1	11.8 ± 0.1
C4	73.2 ± 0.9	142.0 ± 0.6	28.9 ± 1.8	248.7 ± 0.4	38.3 ± 1.1	7.9 ± 0.8
C5	75.5 ± 0.4	99.5 ± 0.8	16.8 ± 2.4	249.6 ± 0.5	50.2 ± 0.4	27.9 ± 1.7
C6	74.0 ± 0.5	145.1 ± 2.4	30.3 ± 0.3	249.4 ± 0.7	39.1 ± 0.3	7.4 ± 0.4
C7	80.3 ± 1.6	102.3 ± 1.1	10.6 ± 2.3	248.4 ± 0.0	49.5 ± 2.7	32.4 ± 2.8
C8	72.7 ± 1.2	147.7 ± 2.4	28.9 ± 0.9	249.5 ± 0.5	40.9 ± 0.2	10.0 ± 0.7

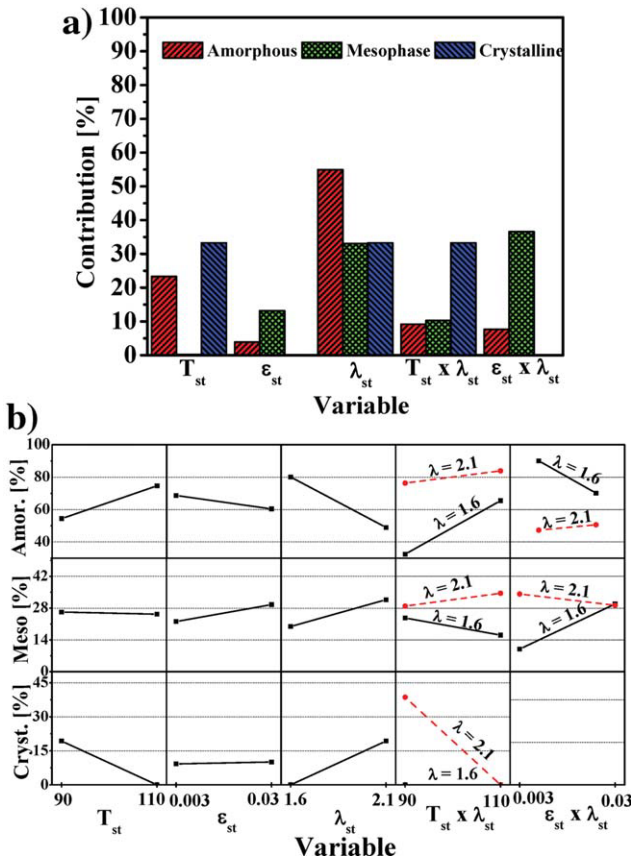

Figure 5 Effect of stretching variables on the amorphous, mesophase, and crystalline-phase mass fractions: (a) percentage of contribution and (b) effects graph. [Color figure can be viewed in the online issue, which is available at wileyonlinelibrary.com.]

low; this indicated that a network was already formed but had not yet reached its fully extensibility. Thus, this condition might belong to the so-called nucleation stage of SDM.[29]

3. Among all, condition C7 presented the highest crystallinity, with third crystallite order, and the highest orientation level. The reason for this was the conjugation of the stretching conditions: lower T_{st}, higher strain rate, and higher λ_{st}. This result might indicate that a crystalline network formed, and the full extensibility of the chains was attained because the levels of orientation were very high for the amorphous phase, f_{av} and Δn (compared to C5). C7 might have been in the growth stage of SDM.[29]

Statistical influence of the stretching variables on the structural development

The statistical influence of the stretching variables on the structure and thermal parameters studied are shown in terms of the percentage contribution and effect graphs. Figure 5 shows the effect of the processing variables on the amorphous-phase, mesophase, and crystalline-phase mass fractions. Figure 6 presents the effects on the orientation functions, and Figure 7 depicts the effects on χ_c, T_g, and T_{cc}.

Phase mass fractions

The most relevant variables to the amount of amorphous phase were λ_{st} and T_{st}, with percentage of contributions of 54 and 23%, respectively [Fig. 5(a)]. However, the mesophase fraction was influenced mainly by λ_{st} and its interactions with $\dot{\varepsilon}_{st}$ (with contributions of 33 and 37%, respectively). The crystalline phase was determined mainly by T_{st}, λ_{st}, and interactions between them (33% each), although only two conditions revealed a crystalline structure. These results revealed the complex effect of the stretching variables on the development of the different phases. Interestingly, the influence of λ_{st} was common to all phase mass fractions. Chain extensibility seemed to govern the development of the

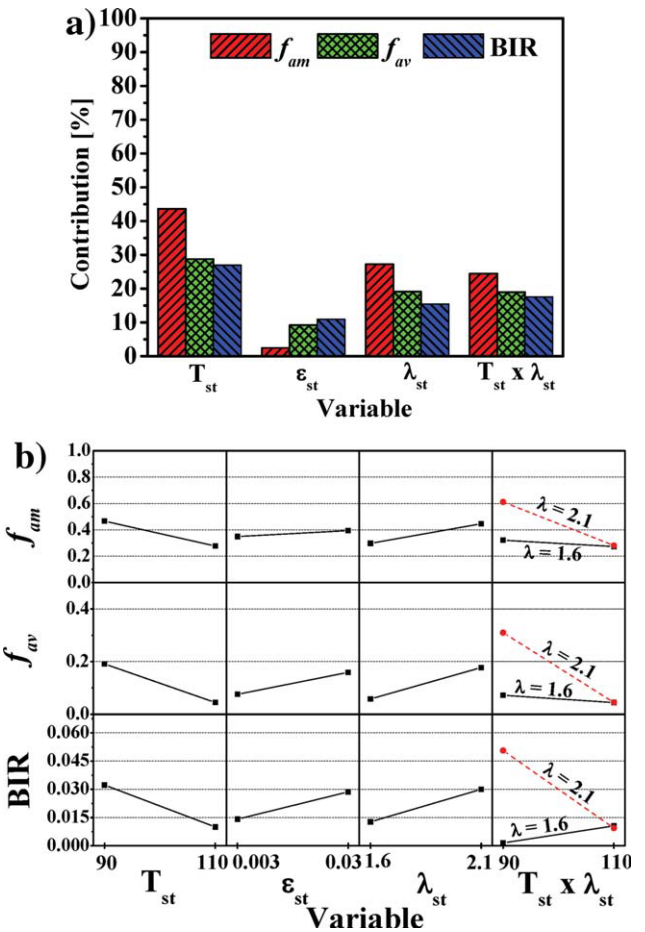

Figure 6 Effect of stretching variables on the level of f_{am}, level of f_{av}, and Δn: (a) percentage of contribution and (b) effects graph. [Color figure can be viewed in the online issue, which is available at wileyonlinelibrary.com.]

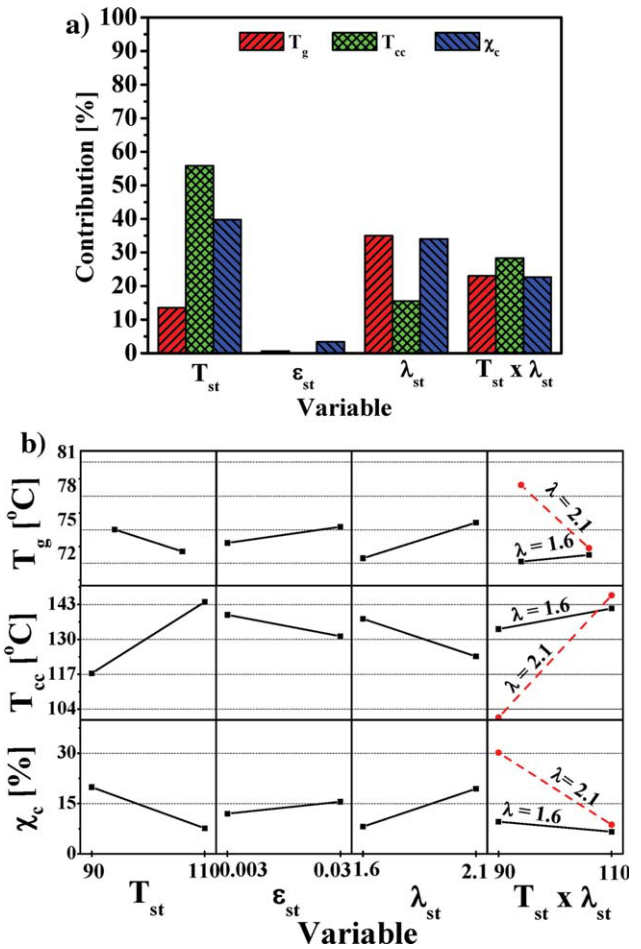

Figure 7 Effect of the stretching variables on T_g, T_{cc}; and χ_c (calculated from DSC): (a) percentage of contribution and (b) effects graph. [Color figure can be viewed in the online issue, which is available at wileyonlinelibrary.com.]

phase fractions, mainly the amount of amorphous material, which was also influenced by chain relaxation (T_{st} effect). The same phenomena determined the amount of crystalline phase, but a higher interaction between these factors was present.

Figure 5(b) presents the graphs corresponding to the effects of the stretching variables upon the phase development. A higher T_{st} favored a high amount of amorphous phase but reduced the amount of the crystalline phase. This may have been caused by the domination of polymer chain relaxation during stretching.[9,14,17,26,40] On the other hand, T_{st} negligibly affected the mesophase development. The opposite effect of chain extensibility and relaxation seemed to govern the development of the amorphous and crystalline phases. High $\dot{\varepsilon}_{st}$ values led to a slight decrease in the amount of amorphous phase, a small increase in the mesophase, and no changes in the amount of crystalline phase. In fact, for low $\dot{\varepsilon}_{st}$ values, when $\dot{\varepsilon}_{st}$ was comparable with chain reptation rate, crystallization was prevented.[38,61] Furthermore, the transformation of the amorphous phase into mesophase was favored by the increase in $\dot{\varepsilon}_{st}$. However, this stretching variable showed a lower effect on the structural development (in the selected range of variation). Increasing λ_{st} resulted in a low amount of amorphous phase, a higher mesophase content, and a higher χ_c. The transformation of the amorphous phase into mesophase was positively affected by the increase in λ_{st}.[40,53] It has been also observed that the initiation of the nucleation stage, where crystalline structures occur, is anticipated by decreasing T_{st} and that a greater amount of strain-induced crystallinity was observed at elevated λ_{st} values.[9,14,17,26] Interactions between T_{st} and λ_{st} supported the effect of the temperature and even amplified it but in a different way. At low λ_{st}, the effect of temperature on the development of the amorphous phase was enhanced. At high λ_{st}, an increase in T_{st} significantly decreased the amount of crystalline phase. In fact, a sufficient level of molecular orientation, imposed by a high λ_{st}, was necessary to start the crystallization process, which competed with a higher chain relaxation with increased temperature.[14,36,39] A statistically important interaction between $\dot{\varepsilon}_{st}$ and T_{st} was found only for the amorphous and mesophase development, which confirmed negligible effect of $\dot{\varepsilon}_{st}$ on the crystalline-phase development. At low λ_{st}, the increase in $\dot{\varepsilon}_{st}$ facilitated the transformation of the amorphous phase into the mesophase, with the opposite effect being observed at elevated λ_{st}.

Molecular orientation

Figure 6 depicts the relevance of the stretching variables on the polymer orientation, namely, on f_{am}, f_{av}, and Δn. In descending order of their statistical significance were T_{st}, λ_{st}, the interactions of T_{st} and λ_{st}, and of less importance, $\dot{\varepsilon}_{st}$ [Fig. 6(a)]. Interestingly, the relevant contribution of the interactions between T_{st} and λ_{st} was that the effect of T_{st} depended on the level of λ_{st}.

Figure 6(b) depicts the dependence of the molecular orientation measurements on the significant stretching parameters and interactions. The variations were similar for all of the molecular orientation data. An increase in T_{st} caused a decrease in the molecular orientation, which was attributed to a higher macromolecular relaxation. An increase in $\dot{\varepsilon}_{st}$ led to a slight increase in the orientation level. In fact, a low $\dot{\varepsilon}_{st}$ promoted the enhancement of the relaxation process due to the longer timescale of the deformation.[14,29,50] An increase of λ_{st} caused the orientation level to rise in contract to its effect on T_{st}. The influence of T_{st} on the orientation level was intensified for high λ_{st} values. Stretching at a high ratio and low temperature was favorable for obtaining a

TABLE IV
Effect of the Stretching Variables on All of the Assessed Parameters

	Parameter								
Variable	Amorphous-phase fraction (%)	Mesophase fraction (%)	Crystalline fraction (%)	f_{am}	f_{av}	BIR	T_g (°C)	T_{cc} (°C)	χ_c (%)
T_{st}	↑↑	↔	↓↓	↓↓	↓↓	↓↓	↓	↑↑	↓↓
$\dot{\varepsilon}_{st}$	↓	↑	↔	↔	↑	↑	↔	↔	↔
λ_{st}	↓↓	↑↑	↑	↑	↑↑	↑	↑	↓	↑↑
$T_{st} \times \lambda_{st}$	↑↑	↓↑	−↓	−↓	−↓	↑↓	−↓	↑↑	↓↓
$\dot{\varepsilon}_{st} \times \lambda_{st}$	↓↑	↑↓	−	−	−	−	−	−	−

In bold are the main contributing factors. Double arrows in the factor cells indicate a strong effect. For interactions, the arrow size is related to the importance of the variation. Horizontal arrows indicate no influence. Stretching variables: $T_{st} \times \lambda_{st}$ = temperature–ratio interaction; $\dot{\varepsilon}_{st} \times \lambda_{st}$ = rate–ratio interaction.

highly oriented PET because of the reduction of chain relaxation and increased chain extension level. Nevertheless, it is widely believed that the orientation level increases with increasing $\dot{\varepsilon}_{st}$ and decreasing temperature.[14,29,50]

Transition temperatures and χ_c

Figure 7(a) shows the percentage contribution of the stretching variables on the transition temperatures (T_g and T_{cc}), as obtained by DSC. T_g was mainly influenced by λ_{st} and its interactions with T_{st}, whereas T_{st} by itself had a relatively small effect (of 15%). The amount of amorphous phase was determined largely by λ_{st} [Fig. 5(a)], and the level of orientation of the amorphous phase was determined by T_{st}, λ_{st}, and their interactions [Fig. 6(a)]. The net result of the opposed effects of these variables [Figs. 5(b) and 6(b)] made T_g mainly dependent on λ_{st} and its interactions with temperature; this highlighted the contribution of the amount of amorphous phase on glass transition. T_{cc} was mainly determined by T_{st}, with less effect by the interaction temperature–ratio and particularly by λ_{st}. This reflected the contribution of the molecular orientation and χ_c on T_{cc}. χ_c was mainly determined, in descending order of importance, by T_{st}, λ_{st}, and their interactions. The contribution of the stretching variables was similar to those assessed by X-rays [Fig. 5(a)], as was expected. As a general trend, $\dot{\varepsilon}_{st}$ had no statistical importance on the variations of these thermal parameters.

According to Figure 7(b), a higher T_{st} decreased T_g, and an increase in λ_{st} shifted it toward higher temperatures. These variations were similar to those of f_{am} [Fig. 6(b)] and opposite to those of χ_c [Fig. 5(b) and 7(b), respectively]. The imposition of a low T_{st} and high λ_{st} led to an increase in the glass-transition values because of a high restraint on the molecular mobility originated by a high χ_c and a high level of molecular orientation.[57] T_{cc} increased with increasing T_{st} in a well-known effect, concomitant with the decrease in ΔH_{cc}.[7,30] Furthermore, at high λ_{st}, the influence of T_{st} was amplified. The same variation of the stretching parameters caused a decrease in T_{cc} (as opposed to the changes in T_g). The effect of the level of the amorphous molecular orientation (noncrystallized samples) on T_{cc} was reported elsewhere: it decreased toward the glass transition as f_{am} increased.[25,59] Again, at high λ_{st}, the influence of T_{st} on T_{cc} was enhanced strongly. The effect of the stretching parameters on χ_c was similar to the previously discussed effects for Figure 5(b): a higher T_{st} decreased the crystallinity because of the predomination of polymer chain relaxation; at high λ_{st}, this variation was enhanced (interaction effect); an increased λ_{st} increased χ_c.

Table IV summarizes the main effects of the stretching variables on all of the assessed parameters. In general, T_{st} and λ_{st} were the main influencing variables; together with their interactions. $\dot{\varepsilon}_{st}$ had a negligible effect.

CONCLUSIONS

With variations of the stretching variables, different PET morphologies were developed; they ranged from quasi-amorphous to semicrystalline states. T_{st} and λ_{st} both had important roles on the structural development. High temperatures hindered the strain-induced crystallization mechanism of PET. This was the result of two possible competing mechanisms: chain elongation due to mechanical deformation and chain relaxation due to the elevated temperature. λ_{st} had a pronounced influence on the strain-induced crystalline phase, mainly when low temperatures were applied. In this way, deformation at a low λ_{st} and high temperatures gave rise to the highest amount of amorphous-phase fraction. In contrast, a decreasing T_{st} facilitated the strain-induced structural development. Structural characterization showed that a semicrystalline morphology was

developed only in conditions that combined a high λ_{st} and low temperature. A combination of low T_{st}, higher strain rate, and higher λ_{st} led to a high χ_c.

In general, a low λ_{st} resulted in a low average polymer chain orientation and, hence, a low Δn. The combination of high λ_{st} and high temperatures resulted in samples with similarly low orientation levels. The use of a high λ_{st} seemed to have a positive influence on the transformation of the amorphous-phase fraction into the mesophase.

The highest crystalline PET showed the highest T_g; this suggested that the crystalline phase geometrically constrained the amorphous phase, inhibiting the amorphous-phase motions. There was an important effect of T_{st} on T_{cc} and, consequently, on the orientation of the amorphous phase.

Statistical analysis indicated the following main effects of the stretching variables on the structural and thermal parameters: (1) the transformation of amorphous phase into the mesophase was mainly controlled by λ_{st} and interactions between λ_{st} and $\dot{\varepsilon}_{st}$; (2) strain-induced crystallization, measured by WAXS and DSC, was governed by T_{st}, λ_{st}, and their interactions; (3) the level of molecular orientation, f_{av} and Δn, was influenced mainly by T_{st}, assisted by λ_{st} and their interactions with similar portions; (4) T_g depended on the orientation level of the amorphous phase, which was governed by λ_{st} and its interactions with temperature, whereas the temperature influence by itself was statistically small; and (5) the dominating influence over T_{cc} was associated with T_{st}, followed by λ_{st} and their interactions.

References

1. Fakirov, S. Handbook of Thermoplastic Polymers: Homopolymers, Copolymers, Blends, and Composites; Wiley-VCH: Weinheim, 2002.
2. Salem, D. R. Polymer 1995, 36, 3605.
3. Goschel, U. Polymer 1995, 36, 1157.
4. Goschel, U.; Urban, G. Polymer 1995, 36, 3633.
5. Goschel, U.; Deutschert, K.; Abetzt, V. Polymer 1996, 37, 1.
6. Goschel, U. Polymer 1996, 37, 4049.
7. Martins, C. I.; Cakmak, M. Polymer 2007, 48, 2109.
8. Salem, D. R. Polymer 1992, 33, 3189.
9. Salem, D. R. Polymer 1992, 33, 3182.
10. Clauss, B.; Salem, D. R. Polymer 1992, 33, 3193.
11. Ajji, A.; Cole, K. C.; Dumoulin, M. M.; Brisson, J. Polymer 1995, 36, 4023.
12. Hermanutz, F.; Salem, D. R.; Wesson, S. P. Polymer 1994, 35, 4611.
13. le Bourvellec, G.; Monnerie, L.; Jarry, J. P. Polymer 1986, 27, 856.
14. le Bourvellec, G.; Monnerie, L.; Jarry, J. P. Polymer 1987, 28, 1712.
15. Nevalainen, K. M. D.; Everall, N. J.; Kuusipalo, J. Mater Chem Phys 2007, 101, 103.
16. Ward, I. M.; Bleackley, M.; Taylor, D. J. R.; Cail, J. I.; Stefto, R. F. T. Polym Eng Sci 1999, 12, 2335.
17. Ajji, A.; Guevremont, J.; Cole, K. C.; Dumoulin, M. M. Polymer 1996, 37, 3707.
18. Ajji, A.; Cole, K. C.; Dumoulin, M. M.; Ward, I. M. Polym Eng Sci 1997, 37, 1801.
19. Keum, J. K.; Song, H. H. Polymer 2005, 46, 939.
20. Matthews, R. G.; Ajji, A.; Dumoulin, M. M.; Prud'homme, R. E. Polymer 2000, 41, 7139.
21. Pearce, R.; Cole, K. C.; Ajji, A.; Dumoulin, M. M. Polym Eng Sci 1997, 37, 1795.
22. Smith, M. R.; Cooper, S. J.; Winter, D. J.; Everall, N. Polymer 2006, 47, 5691.
23. Chevalier, L. M. Y. Mech Mater 2007, 39, 596.
24. Adams, A. M.; Buckley, C. P.; Jones, D. P. Polymer 2000, 41, 771.
25. Gowd, E. B.; Ramesh, C.; Byrne, M. S.; Murthy, N. S.; Radhakrishnan, J. Polymer 2004, 45, 6707.
26. Salem, D. R. Polymer 1994, 35, 771.
27. Morawiec, J.; Bartczak, Z.; Pluta, M.; Galeski, A. J Appl Polym Sci 2002, 86, 1426.
28. Vigny, M.; Tassin, J. F.; Gibaud, A.; Lorentz, G. Polym Eng Sci 1997, 11, 1785.
29. Gorlier, E.; Haudin, J. M.; Billon, N. Polymer 2001, 42, 9541.
30. Dargent, E.; Grenet, J.; Dahoun, A. Polym Eng Sci 1997, 37, 1853.
31. Venkatesvaran, H.; Cakmak, M. Polym Eng Sci 2001, 2, 341.
32. Ajji, A.; Guevremont, J.; Matthews, R. G.; Dumoulin, M. M. J Plast Film Sheeting 1999, 15, 256.
33. Engelaere, J. C.; Cavrot, J. P.; Rietsch, F. Polymer 1982, 23, 766.
34. Natu, A. A.; Lofgren, E. A.; Jabarin, S. A. Polymer Eng Sci 2005, 45, 400.
35. Morawiec, J.; Bartczak, Z.; Pluta, M.; Galeski, A. J Appl Polym Sci 2002, 86, 1426.
36. Mahendrasingam, A.; Martin, C.; Fuller, W.; Blundell, D. J.; Oldman, R. J.; Harvie, J. L.; MacKerron, D. H.; Riekel, C.; Engstrom, P. Polymer 1999, 40, 5553.
37. Blundell, D. J.; Mahendrasingam, A.; Martin, C.; Fuller, W.; MacKerron, D. H.; Harvie, J. L.; Oldman, R. J.; Riekel, C. Polymer 2000, 41, 7793.
38. Mahendrasingam, A.; Blundell, D. J.; Martin, C.; Fuller, W.; MacKerron, D. H.; Harvie, J. L.; Oldman, R. J.; Riekel, C. Polymer 2000, 41, 7803.
39. Blundell, D. J.; MacKerron, D. H.; Fuller, W.; Mahendrasingam, A.; Martin, C.; Oldman, R. J.; Rule, R. J.; Riekel, C. Polymer 1996, 37, 3303.
40. Chaari, F.; Chaouche, M.; Doucet, J. Polymer 2003, 44, 473.
41. Chaari, F.; Chaouche, M. J Polym Sci Part B: Polym Phys 2004, 42, 1915.
42. Kolb, R.; Seifert, S.; Stribeck, N.; Zachmann, H. G. Polymer 2000, 41, 2931.
43. Kawakami, D.; Ran, S.; Burger, C.; Fu, B.; Sics, I.; Chu, B.; Hsiao, S. B. Macromolecules 2003, 36, 9275.
44. Middleton, A. C.; Duckett, R. A.; Ward, I. M.; Mahendrasingam, A.; Martin, C. J Appl Polym Sci 2001, 79, 1825.
45. Kawakami, D.; Ran, S.; Burger, C.; Avila-Orta, C.; Sics, I.; Chu, B.; Benjamin, S. H.; Kikutani, T. Macromolecules 2006, 39, 2909.
46. Mahendrasingam, A.; Martin, C.; Fuller, W.; Blundell, D. J.; Oldman, R. J.; MacKerron, D. H.; Harvie, J. L.; Riekel, C. Polymer 2000, 41, 1217.
47. Ran, S.; Wang, Z.; Burger, C.; Chu, B.; Hsiao, B. S. Macromolecules 2002, 35, 10102.
48. Asano, T.; Balta Calleja, F. J.; Flores, A.; Tanigaki, M.; Mina, M. F.; Sawatari, C.; Itagaki, H.; Takahashi, H.; Hatta, I. Polymer 1999, 40, 6475.
49. Kawakami, D.; Hsiao, B. S.; Ran, S.; Burger, C.; Fu, B.; Sics, I.; Chu, B.; Kikutani, T. Polymer 2004, 45, 905.
50. Oultache, A. K.; Kong, X.; Pellerin, C.; Brisson, J.; Pezolet, M.; Prud'homme, R. E. Polymer 2001, 42, 9051.
51. Varma, P.; Lofgren, E. A.; Jabarin, S. A. Polym Eng Sci 1998, 38, 245.

52. Varma, P.; Lofgren, E. A.; Jabarin, S. A. Polym Eng Sci 1998, 38, 237.
53. Llana, P. G.; Boyce, M. C. Polymer 1999, 40, 6729.
54. Roy, R. K. Design of Experiments Using the Taguchi Approach; Wiley: New York, 2001.
55. Stribeck, N. X-Ray Scattering of Soft Matter; Springer: Berlin, 2007.
56. Yang, H. H.; Chouinard, M. P.; Lingg, W. J. J Polym Sci Part A-2: Polym Phys 1982, 20, 981.
57. Viana, J. C.; Alves, N. M.; Mano, J. F. Polym Eng Sci 2004, 44, 2174.
58. Arnoult, M.; Dargent, E.; Mano, J. F. Polymer 2007, 48, 1012.
59. Alves, N. M.; Mano, J. F.; Balaguer, E.; Meseguer Duenas, J. M.; Gomez Ribelles, J. L. Polymer 2002, 43, 4111.
60. Martins, C. I.; Cakmak, M. Macromolecules 2005, 38, 4260.
61. Blundell, D. J.; Oldman, R. J.; Fuller, W.; Mahendrasingam, A.; Martin, C.; MacKerron, D. H.; Harvie, J. L.; Riekel, C. Polym Bull 1999, 42, 357.